molbank

MDPI

Communication

N-Demethyl-*N*-nitrosolevofloxacin

Claudio Maestri [1,2], Mattia Lopresti [3], Ivana Miletto [1], Attila Benyei [4], Marzia Petreti [1], Luisa Zangirolami [2], Camilla Cavallotti [5] and Giovanni B. Giovenzana [1,*]

[1] Dipartimento di Scienze del Farmaco, Università del Piemonte Orientale, Largo Donegani 2, 28100 Novara, Italy
[2] PRC Ticinum Lab S.r.l., Via Bovio 6, 28100 Novara, Italy
[3] Dipartimento di Scienze e Innovazione Tecnologica, Università del Piemonte Orientale, Via T. Michel 11, 15121 Alessandria, Italy
[4] Department of Physical Chemistry, University of Debrecen, Egyetem tér 1, H-4032 Debrecen, Hungary
[5] CAGE Chemicals S.r.l., Via Bovio 6, 28100 Novara, Italy
* Correspondence: giovannibattista.giovenzana@uniupo.it; Tel.: +39-(0)321375846

Abstract

Levofloxacin is an antibiotic belonging to the fluoroquinolone family. *N*-Demethyllevofloxacin, a metabolite and an impurity of levofloxacin, features a secondary amine that is susceptible to *N*-nitrosation, raising concerns about the formation of a potentially toxic nitrosamine. The corresponding *N*-nitrosamine was synthesized in two steps and characterized using HRMS, NMR spectroscopy, IR spectroscopy, UV absorption and emission spectroscopies and powder X-ray diffraction. This work provides a reliable reference for the quantitation and control of nitrosamine impurities associated with levofloxacin in chemical and pharmaceutical contexts.

Keywords: levofloxacin; nitrosamines; XRPD; crystal structure

1. Introduction

Nitrosamines, classified under ICH M7 as Class 1 mutagenic impurities [1], arise via nitrosation of secondary/tertiary amines and occur as either small-molecule contaminants or nitrosamine drug substance-related impurities (NDSRIs) formed from Active Pharmaceutical Ingredient (API)-embedded amines. Root causes span from reagents/solvents to excipients, process conditions, cross-contamination, and storage-driven degradation [2]. Their carcinogenicity stems from CYP-mediated α-hydroxylation that generates DNA-reactive species, prompting stringent oversight: recent FDA guidance introduces the Carcinogenic Potency Categorization Approach (CPCA) for acceptable intake limits, while EMA updates emphasize proactive risk mitigation, precursor control, and lot-specific testing [3]. Meeting the ultralow limits demands high-specificity, high-sensitivity methods: GC-MS for volatile, low-MW nitrosamines (often with derivatization and selective cleanup) and LC-MS/MS, preferably in MRM mode, for non-volatile or API-like NDSRIs, aligned with ICH Q2(R2) validation [4]. The absence of certified NDSRI standards is a persistent and urgent issue, prompting in-house synthesis/characterization under stringent safety criteria due to probable human carcinogenicity, and reinforcing the need for end-to-end risk assessment across manufacturing and lifecycle control.

Levofloxacin (Scheme 1) is a third-generation fluoroquinolone antibiotic and the active *L*-isomer of ofloxacin, structurally defined as (–)-(*S*)-9-fluoro-2,3-dihydro-3-methyl-10-(4-methylpiperazin-1-yl)-7-oxo-7*H*-pyrido [1,2,3-de][1,4]benzoxazine-6-carboxylic acid. Its tricyclic quinolone core, bearing a fluorine atom and a *N*-methylpiperazinyl residue, confers

Academic Editor: Nicholas Leadbeater

Received: 30 June 2026
Revised: 28 July 2026
Accepted: 31 July 2026
Published: 4 August 2026

broad-spectrum activity against Gram-positive and Gram-negative bacteria by inhibiting DNA gyrase and topoisomerase IV, enzymes essential for bacterial DNA replication [5]. Clinically, levofloxacin is administered orally or intravenously, showing high bioavailability and extensive tissue penetration, making it effective in respiratory tract infections, urinary tract infections, skin and soft tissue infections, and certain multidrug-resistant tuberculosis cases [6]. As with other APIs containing secondary or tertiary amines, levofloxacin may be susceptible to the formation of nitrosamine drug substance-related impurities (NDSRIs), which are recognized as mutagenic and potentially carcinogenic, prompting regulatory agencies such as the FDA and EMA to implement strict risk assessment and control measures in its manufacture and storage.

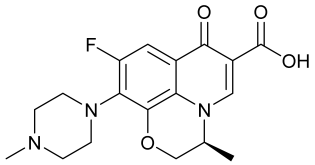

Scheme 1. Levofloxacin.

In this work we describe the synthesis of *N*-demethyl-*N*-nitrosolevofloxacin and the comprehensive structural characterization of this *N*-nitrosamine, an NDSRI of levofloxacin, representing a standard for the analytical determination of this specific compound in the commercially available formulations of this important API.

2. Results and Discussion

2.1. Synthesis

The synthesis of *N*-demethyl-*N*-nitrosolevofloxacin (**3**) is described in Scheme 2. The commercially available (*S*)-difluoroquinolone (**1**) undergoes selective nucleophilic aromatic substitution of a single fluorine atom, driven by the electron-withdrawing effect of the *para*-ketone group. Heating the starting material (**1**) in DMSO with a slight excess of piperazine led to the formation of *N*-demethyllevofloxacin (**2**) in 60% yield. Treatment of compound (**2**) with sodium nitrite in a water/acetic acid mixture allowed for the clean introduction of the *N*-nitroso group (87% yield).

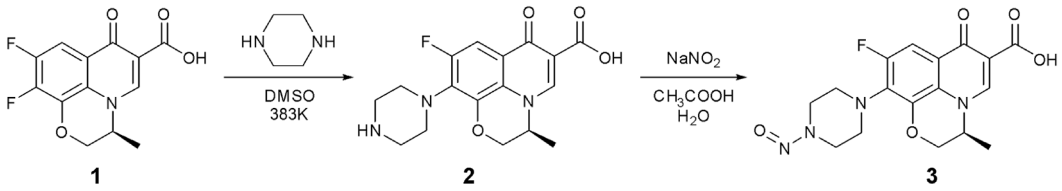

Scheme 2. Synthesis of *N*-demethyl-*N*-nitrosolevofloxacin (**3**).

2.2. X-Ray Crystal Structure(s)

N-Demethyl-*N*-nitrosolevofloxacin (**3**) could be obtained in microcrystalline form by recrystallization from different solvents, including acetonitrile, 1-butanol, 1,2-propanediol and water (very low solubility). Because of this nature, structure solution was carried out using X-ray powder diffraction (XRPD) data resulting in a structural model named **3α**.

Compound **3α** crystallizes in the monoclinic crystal system in the $P2_1$ space group. The unit-cell parameters, reported along with other crystallographic details in Table 1, are a = 13.145(6)Å, b = 6.949(2)Å, c = 9.890(3)Å, and β = 111.423(17)°, giving a unit-cell volume of V = 841.0(5)Å^3. With Z = 2, the structure is relatively compact, with an average atomic volume of 15.57Å^3 per atom, which is slightly lower than the empirical value commonly

used as a rule of thumb for organic crystal structures (ca. 18Å^3 per atom). The asymmetric unit and packings along the *b*-axis and the *c*-axis are reported in Figure 1a–c.

Table 1. Crystal data, data collection and structure refinement details of structures **3α** and **3β**.

Compound	**3α**	**3β**
Empirical formula	$C_{17}H_{17}FN_4O_5$	$C_{17}H_{17}FN_4O_5$
Formula weight	376.342 g mol^{-1}	376.342 g mol^{-1}
Temperature	298(2)K	298(2)K
Wavelength	1.54059Å	0.71073Å
Crystal system	Monoclinic	Monoclinic
Space group	$P2_1$ (4)	$C2$ (5)
Unit-cell dimension	a = 13.145(6)Å	a = 17.515(9)Å
	b = 6.949(2)Å	b = 7.116(3)Å
	c = 9.890(3)Å	c = 17.524(8)Å
	β = 111.64(2)°	β = 118.31(6)°
Volume	841.0(5)Å^3	1922.7(9)Å^3
Z	2	4
Density (calculated)	1.486 g cm^{-3}	1.300 g cm^{-3}
Absorption coefficient	1.011 mm^{-1}	0.104 mm^{-1}
Crystal habit	Powder	Acicular
Theta range for data collection	1.00–45.00°	3.15–20.80°
Independent reflections	-	1762 [R_{int} = 0.067]
Completeness to theta = 20.8°	-	99.55%
Goodness-of-fit on F^2	-	1.1224
Final R indices	Rietveld:	[I > 2σ (I)]:
		R_1 = 0.1220
		wR_2 = 0.2957
	R = 0.07657	
	R_{wp} = 0.11371	All data:
		R_1 = 0.1754
		wR_2 = 0.3496

Compact packing can be primarily attributed to π-π stacking interactions and to steric constraints imposed by the molecular geometry of **3**. The π-π stacking occurs between the fused aromatic ring systems, which are arranged in parallel head-to-tail columns. Because of the symmetry operations of the space group, adjacent columns are oriented in opposite directions, resulting in an almost orthogonal arrangement between stacked N4–C9–C10–C11–C12–C13 ring systems. The angle defined by atom N4 and the centroids of the interacting rings is 94.4°, while the interplanar centroid–centroid separation is 3.555Å (Figure 1c). Steric hindrance forces the N-nitrosopiperazyl moiety to adopt a conformation rotated by 77.5° with respect to the plane of the tricyclic quinolone ring system. The nitrosamine group was restrained to remain coplanar with the piperazine ring during refinement, consistent with the conformation observed in related crystal structures

reported in the literature (CSD Version 6.01 Update 2025, November; CCDC Codes: IRUFIO, ANEVUO) [7].

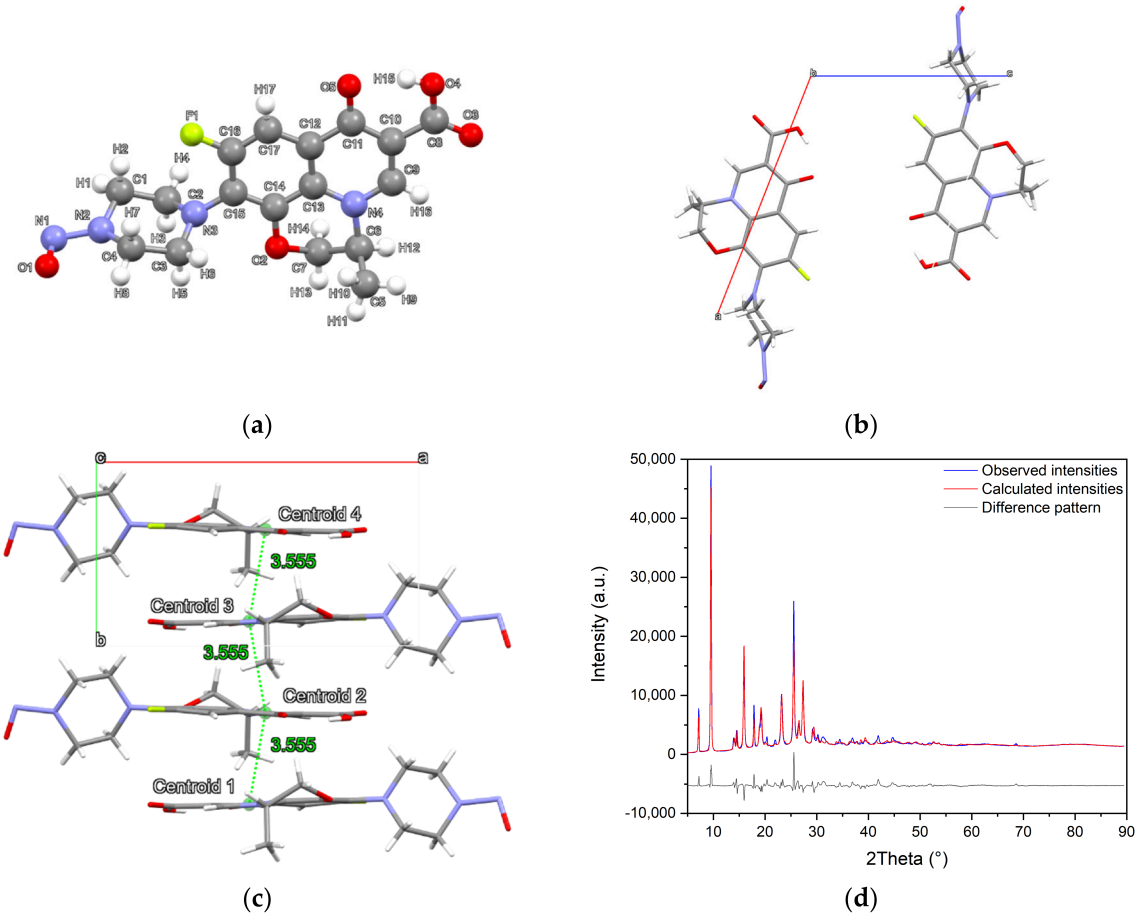

Figure 1. Structural views and refinement of **3*α***. (**a**) Asymmetric unit. (**b**) Packing along the b-axis. (**c**) Packing along the *c*-axis and detail of the π-π stacking interaction in the structure. (**d**) Final Rietveld refinement.

The nitrosamine moiety is directed toward the carboxylic hydroxyl group of a neighboring molecule within the same head-to-tail column, resulting in a close intermolecular contact (N1—O1···H15 = 2.567Å, N1—O1···H15 angle = 86.33°). Because of the head-to-tail molecular arrangement, the crystal packing viewed along the *c*-axis (Figure 1c) displays two distinct alternating regions: one enriched in *N*-nitrosopiperazyl groups and the other dominated by π-π stacking interactions between adjacent molecular columns. A search of the Cambridge Structural Database (Version 6.01 Update November, 2025) resulted in 25 hits for *N*-nitrosopiperazyl derivatives, and the average N-N-O angle is 115 degrees, while in structure **3*α*** the corresponding data is 100 degrees. The structure is also stabilized with an intramolecular hydrogen bond between the carboxylic acid proton and the benzoxazine carbonyl moiety (see Supplementary Materials). Analysis of the symmetry of the structure using the ADDSYM routine implemented in CheckCIF suggested the presence of a possible higher-symmetry arrangement, with an approximate fit of 88%. However, the suggested higher-symmetry description would require an inversion center and therefore a racemic arrangement of the molecules. Since compound **3** is a single enantiomer, such a symmetry description is chemically impossible. Therefore, the structure is correctly described in the non-centrosymmetric space group $P2_1$. Furthermore, given the powder nature of the data, attempts to model inversion twinning within $P2_1$ did not lead to any improvement in the Rietveld refinement profile factors, confirming the validity of the untwinned model.

The Rietveld refinement reported in Figure 1d demonstrates good agreement between the observed and calculated diffraction patterns, also confirmed by the agreement parameters reported in Table 1. The difference pattern highlights residual discrepancies associated primarily with the most intense reflections, which are attributed to preferred orientation effects. Despite the precautions adopted during sample preparation, these effects could not be completely eliminated. Preferred orientation effects were attenuated using a March–Dollase correction along the [010] direction. To assess the robustness of the crystallographic model, independent simulated annealing runs initiated from random molecular positions and orientations were performed using diffraction patterns collected from separately recrystallized samples. In all cases, the calculations converged to the same structural model, providing strong evidence for the reliability of the solution.

Additional reflections attributable to a minor impurity phase were observed in the 1-butanol-recrystallized sample (Figure 2a). The sharper extra peaks indicated the presence of a crystalline phase with a larger crystal size and a larger unit cell. Under the optical microscope, the impurity was identified as small rod-shaped crystals approximately 20 µm in length. Several single-crystal X-ray diffraction experiments were carried out on these crystals, in the attempt of indexing such an extra phase.

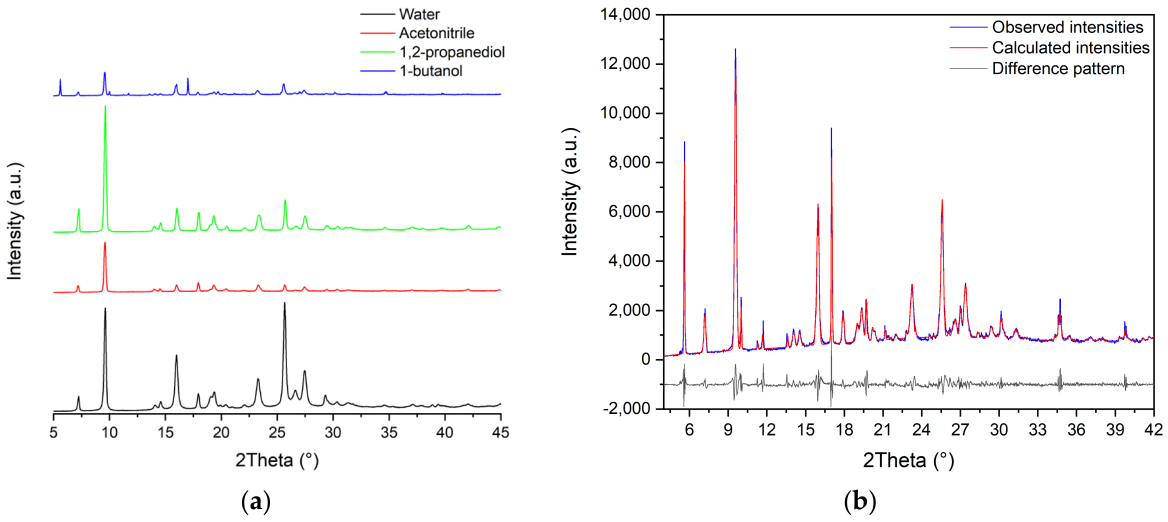

(**a**) (**b**)

Figure 2. (**a**) Comparison between XRPD patterns collected on **3** samples recrystallized with different solvents. In the 1-butanol-recrystallized pattern (blue curve), extra reflections due to the presence of phase **3β** can be observed. (**b**) Pawley fit performed on 1-butanol-recrystallized sample's XRPD pattern using both **3*α*** and **3β** structures.

The impurity was subsequently identified as a polymorphic form of **3**. This polymorph ("**3β**") crystallizes in the monoclinic crystal system in the C2 space group, with unit-cell parameters a = 17.515(9)Å, b = 7.116(3)Å, c = 17.524(8)Å, and β = 118.31(6)°. The unit-cell volume is V = 1922.7(19)Å^3 with Z = 4. Compared with the form described above, this polymorph exhibits a lower packing efficiency, corresponding to an average atomic volume of 18.49Å^3 per atom.

The structural model obtained from single-crystal diffraction should be regarded as preliminary because of the limited quality of the diffraction data: the combination of weak diffraction intensity, the lack of reflections at higher resolutions than 1Å, and the small crystal dimensions resulted in suboptimal refinement statistics and several unavoidable level A and B alerts in the CheckCIF report. Consequently, even if the structure has been identified as a polymorph (**3β**), the data quality does not allow for a proper structural discussion of this polymorph in the present work. It is worth noting that potential solvent-accessible voids within the crystal structure of **3β** (measuring approximately 63Å^3 per unit

cell according to Mercury) were evaluated for the presence of disordered solvent in the voids. An exploratory refinement was performed using the SQUEEZE routine (Olex2), which identified a total of 88 electrons in a void volume of 334Å^3 per unit cell. Given the $P2_1$ space group ($Z = 2$), this electron count (ca. 44 electrons per asymmetric unit) is highly consistent with the presence of one disordered molecule of 1-butanol per asymmetric unit. Although applying the SQUEEZE solvent led to a nominal improvement in the agreement factors ($R_1 = 6.97\%$, w$R_2 = 22.01\%$), it introduced severe physical instabilities in the atomic displacement parameters (ADPs). Specifically, several carbon atoms became non-positive-definite (NPD) and the flexible nitrosamine group developed highly distorted, oblate thermal ellipsoids. Consequently, to preserve a physically meaningful and chemically sound description of the molecular framework, the non-squeezed model with stable, positive-definite ADPs was retained for the final structural refinement. Nevertheless, the crystallographic model has been deposited with the CCDC for completeness. While the atomic model should be interpreted with appropriate caution, the unit-cell parameters and space-group assignment are considered reliable. Furthermore, the identification of this phase as an impurity is supported by the Pawley fit of the powder diffraction data collected from the 1-butanol-recrystallized sample using both **3α** and **3β** structures (Figure 2b), which confirms the presence of the polymorphic phase.

D-spacings, along with the squared structure factors for each solved crystal structure, are reported in the ESI (Tables S2 and S3).

2.3. Electronic Spectroscopies

The photophysical properties of *N*-demethyl-*N*-nitrosolevofloxacin were investigated by UV-Vis absorption, fluorescence emission, and excitation spectroscopy. The absorption spectrum (Figure 3, dashed line) exhibits structured bands in the UV region, with a main maximum at about 297 nm and an additional higher-energy contribution around 224 nm, together with a weaker tail extending toward longer wavelengths. Upon UV excitation, the compound displays a broad and essentially structureless emission band centered in the green spectral region, at approximately 495–505 nm, indicating a marked bathochromic shift between absorption and fluorescence maxima (Figure 3, solid line).

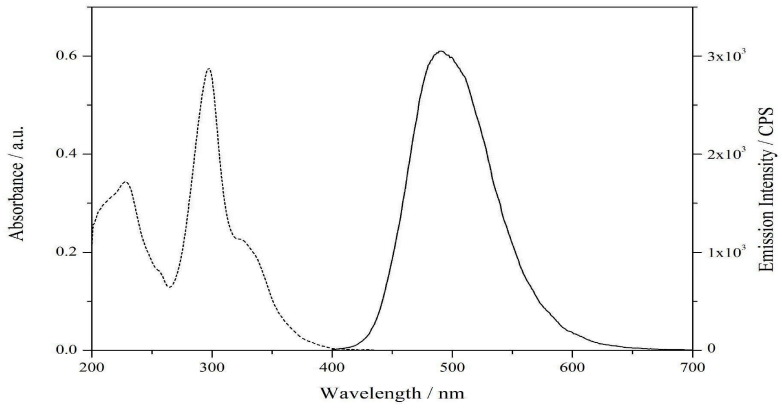

Figure 3. *N*-Demethyl-*N*-nitrosolevofloxacin (**3**) absorption (dashed line) and emission (solid line) spectra. Emission spectrum is obtained upon excitation at 297 nm.

The excitation spectrum (Figure 4) closely reproduces the absorption profile, with prominent features at about 224, 297, and 330 nm, supporting the assignment of the observed fluorescence to the same ground-state absorbing species rather than to a secondary emissive impurity [8]. The large Stokes shift and the broad emission envelope are consistent with the behavior commonly reported for fluoroquinolone-based chromophores [9–11]. In this context, the *N*-nitroso-substituted derivative appears to retain the characteristic

emissive response of the quinolone scaffold, as also observed for intermediate compound **2** (Figures S11 and S12), since the *N*-nitroso group is not directly conjugated with the chromophore and is therefore expected to exert only a limited influence on the electronic transitions.

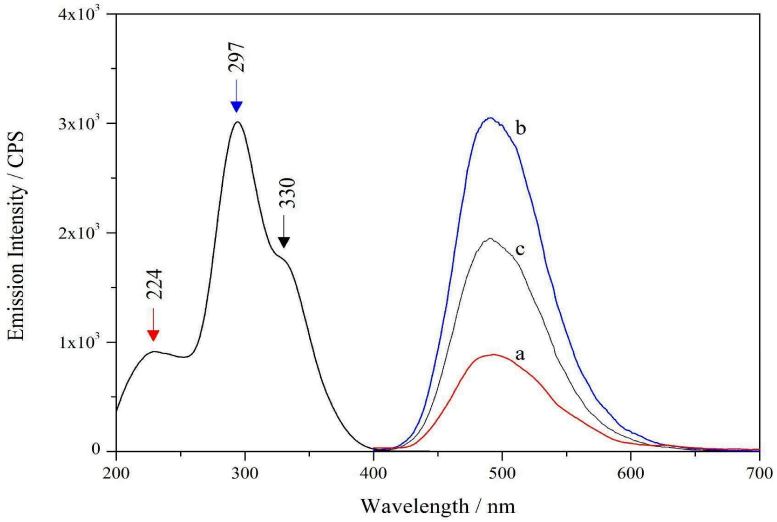

Figure 4. Excitation (black line) and emission spectra of *N*-demethyl-*N*-nitrosolevofloxacin (**3**), obtained upon excitation at 224 nm (a, red curve), 297 nm (b, blue curve) and 330 nm (c, black curve).

3. Materials and Methods

3.1. General

All reagents and solvents were obtained by Carlo Erba (Cornaredo, Italy) and used without purification. The starting material (**1**, *S*-enantiomer) was purchased by BLDpharm (Reinbek, Germany) and used as received. ^{1}H, ^{13}C, and ^{19}F NMR spectra were recorded at 9.4 T on a Bruker Avance Neo 400 spectrometer. Chemical shifts are reported in ppm and referenced to the protic impurities of deuterated solvents (^{1}H), to the center of the multiplet of the deuterated solvents (^{13}C) and to the signal of $CFCl_3$ (^{19}F). High-resolution mass spectra were registered on an Agilent Q-ToF G6546 spectrometer. Attenuated Total Reflection (ATR) Fourier-Transform Infrared (FT-IR) spectra were acquired on a Bruker Alpha II instrument (Bruker Optics, Rosenheim, Germany), equipped with an ATR accessory (monolithic diamond crystal) and a DTGS (Deuterated Triglycine Sulphate) detector. Spectra were registered over 24 scans in the 4000–450 cm^{-1} range at a resolution of 4 cm^{-1}. OPUS Software (Release 8.7) was used for the processing.

WARNING: Nitrosamines are potential carcinogens and reproductive toxins; ensure all handling is restricted to a certified chemical fume hood with appropriate personal protective equipment to prevent inhalation or dermal absorption.

*3.2. N-Demethyllevofloxacin (**2**)*

In a 250 mL round-bottomed flask, (3*S*)-9,10-difluoro-2,3-dihydro-3-methyl-7-oxo-7*H*-pyrido[1,2,3-de]-1,4-benzoxazine-6-carboxylic acid (**1**, 8.00 g, 28.4 mmol) is dissolved in DMSO (80 mL). Piperazine (19.6 g, 228 mmol) is added, and the mixture is stirred at 130 °C for 2 h. The solvent and excess piperazine are removed by distillation/sublimation under vacuum. Methanol (50 mL) is added to the yellow residue, and the mixture is stirred overnight. The crude product is isolated by filtration on a Buchner funnel, recrystallized by 2-propanol/water and dried under vacuum, resulting in an off-white solid weighing 12.8 g (yield 60%).

^{1}H-NMR (DMSO-d_6, 400.2 MHz, 298 K) δ (ppm): 8.95 (s, 1H, H-5), 7.54 (d, 1H, J = 12.4 Hz, H-8), 4.92 (bq, 1H, H-3), 4.59 (bd, 1H, J = 11.0 Hz, H-2), 4.38 (dd, 1H, J_1 = 12.0 Hz, J_2 = 1.9 Hz, H-2), 3.35–3.25 (m, 4H, CH_2-13), 2.95–2.89 (m, 4H, CH_2-14), 1.45 (d, 3H, J = 6.7 Hz, CH_3-11).

^{13}C-NMR (DMSO-d_6, 100.6 MHz, 298 K) δ (ppm): 176.2 (d, J_{CF} = 3.3 Hz, C-7), 165.8 (COOH), 155.4 (C, d, J_{CF} = 246.7 Hz, C-9), 145.9 (CH-5), 140.2 (d, J_{CF} = 6.9 Hz, C-10a), 131.9 (d, J_{CF} = 13.8 Hz, C-10), 124.7 (C-10b), 119.7 (d, J_{CF} = 9.5 Hz, C-7a), 106.7 (C-6), 103.1 (d, J_{CF} = 24.3 Hz, C-8), 68.0 (CH-3), 54.7 (CH_2-2), 50.40 and 50.36 (CH_2-13), 45.4 (CH_2-14), 17.6 (CH_3-11).

^{19}F-NMR (DMSO-d_6, 376.6 MHz, 298 K) δ (ppm): −119.9 (d, J = 12.5 Hz).

HRMS (ESI): m/z calculated for $[M + H]^+$ $C_{17}H_{19}FN_3O_4^+$: 348.1354; found: 348.1354 (Δ = 0.0 ppm).

FTIR (ATR) cm^{-1}: 3500–3200 (peak 3392) br (N–H, piperazine), 3042 w (aromatic C–H), 2980, 2951, 2854 m (aliphatic C–H), 1706 s (C=O, carboxylic acid), 1620 s (conjugated C=O, quinolone), 1500–1520 m (aromatic C=C), 1450–1470 m (CH_2 bending), 1380–1420 m (in-plane O–H/C–H bending), 1330–1350 m (C–N), 1260–1290 m–s (C–O–C/C–F), 1100–1150 s (C–O–C), 970–1000 m (skeletal vibrations), 820–850 m (aromatic C–H out-of-plane), 760–780 s (aromatic C–H out-of-plane), 600–650 m (skeletal deformations).

*3.3. N-Nitroso-N-demethyllevofloxacin (**3**)*

An aqueous solution of sodium nitrite (2.96 g, 42.9 mmol, in 20 mL H_2O) is added dropwise to a solution of compound **2** (3.00 g, 8.64 mmol) in acetic acid/water (30 mL + 30 mL). After the addition the mixture is stirred for a further 6 h. The precipitated product is filtered on a Buchner funnel, washed with 1:1 acetic acid/water, and then dried under vacuum, resulting in an off-white solid weighing 2.83 g (yield 87%).

^{1}H-NMR (DMSO-d_6, 400.2 MHz, 298 K) δ (ppm): 8.98 (s, 1H, H-5), 7.60 (d, 1H, J = 12.0 Hz, H-8), 4.94 (bq, 1H, J = 7.0 Hz, H-3), 4.61 (bd, 1H, J = 11.3 Hz, H-2), 4.41 (dd, 1H, J_1 = 11.2 Hz, J_2 = 2.8 Hz, H-2), 4.36 (dd, 2H, J_1 = 6.6 Hz, J_2 = 4.0 Hz, C$\underline{H_2}$-14), 3.90 (t, 2H, J = 5.3 Hz, C$\underline{H_2}$-14), 3.55 (bt, 2H, J = 5.2 Hz, CH_2-13), 3.29 (bt, 2H, J = 5.5 Hz, CH_2-13), 1.47 (d, 3H, J = 6.7 Hz, CH_3-11).

^{13}C-NMR (DMSO-d_6, 100.6 MHz, 298 K) δ (ppm): 176.3 (d, J_{CF} = 2.9 Hz, C-7), 166.9 (COOH), 155.3 (C, d, J_{CF} = 246.7 Hz, C-9), 146.0 (CH-5), 140.6 (d, J_{CF} = 6.5 Hz, C-10a), 130.9 (d, J_{CF} = 14.5 Hz, C-10), 124.7 (C-10b), 120.4 (d, J_{CF} = 9.4 Hz, C-7a), 107.2 (C-6), 103.1 (d, J_{CF} = 24.0 Hz, C-8), 68.2 (CH-3), 54.8 (CH_2-2), 50.66, 50.63, 50.0, 49.00, 48.96, 40.4 (CH_2-13, CH_2-14), 17.7 (CH_3).

^{19}F-NMR (DMSO-d_6, 376.6 MHz, 298 K) δ (ppm): −120.3 (d, J = 11.9 Hz).

HRMS (ESI): m/z calculated for $[M + H]^+$ $C_{17}H_{18}FN_4O_5^+$: 377.1256; found: 377.1260 (Δ = 1.1 ppm).

FTIR (ATR) cm^{-1}: 3500–2500 br (O–H, carboxylic acid), 3054 w (aromatic C–H), 2992, 2929, 2883, 2842 m (aliphatic C–H), 1724 s (C=O, carboxylic acid), 1620 s (conjugated C=O, quinolone), 1500–1520 m (N=O, N-nitroso, overlapped with aromatic C=C), 1450–1470 m (CH_2 bending), 1380–1420 m (in-plane O–H/C–H bending), 1330–1350 m (C–N), 1260–1290 m-s (C–O–C/C–F), 1100–1150 s (C–O–C), 970–1000 m (skeletal vibrations), 820–850 m (aromatic C–H out-of-plane), 760–780 s (aromatic C–H out-of-plane), 600–650 m (skeletal deformations).

3.4. X-Ray Characterization and Structure Solution

X-ray powder diffraction patterns were collected on a Bruker D8 Advance (Bruker AXS GmbH, Karlsruhe, Germany) diffractometer equipped with Cu Kα (λ = 1.5418Å) radiation and a LynxEye XE-T silicon strip detector (Bruker AXS GmbH, Karlsruhe, Germany). The

instrument goniometer radius was set to 280 mm, and the tube was operated at 40 mA and 40 kV. The diffractometer was used in Bragg–Brentano geometry and the samples were placed in a standard zero-background sample holder. On top of the samples, an air-scatter knife was positioned to reduce noise during low-angle measurements. Both on the primary and secondary optics, Soller slits of 2.5° were used to reduce axial divergence. Variable diverging slits were used as primary optics to ensure a constant illuminated sample length of 17 mm. The diffraction patterns were collected in an angular range from 2° to 90° in 2θ, with a step-size of 0.02° and irradiation time of 0.5 s per step.

Powder diffraction patterns were indexed by EXPO2 version 2.3.9 [12] using the NTREOR09 algorithm [13]. A search of the Cambridge Structural Database using the unit-cell parameters obtained during the indexing confirmed the novelty of the structure. Structure solution was then carried out on the acetonitrile-recrystallized powder by simulated annealing in direct space using EXPO2.

During the screening by X-ray powder diffraction, small crystals were found in the sample recrystallized with 1-butanol. Single-crystal diffraction data were collected on such crystals using an Oxford Xcalibur CCD area detector diffractometer with a graphite monochromator and Mo Kα (λ = 0.71069Å) radiation. Data collection and data reduction were performed using CrysAlisPRO version 44.85 [14]. Single-crystal structure solution was attempted by direct methods using SHELXT version 2018/2 [15] within the Olex2 v1.5 GUI [16]. The following refinement was carried out with full-matrix least-squares employing SHELXT. Hydrogen atoms were placed in the expected positions, with C–H = 0.97 (phenyl) or 0.95–1.00Å (methyl), and refined as riding atoms on their carrier atoms, with U*iso*(HAr) = 1.2U*eq*(C) for aromatic H atoms and U*iso*(HMe) 1.5U*eq*(C) for methyl H atoms.

Crystal data, data collection and structure refinement details for both structures are summarized in Tables 1 and S1.

Structural figures were prepared using CCDC Mercury 2025.3.3 [17]. The crystallographic information file (CIF) containing the final structural models have been deposited within the Cambridge Crystallographic Data Centre (CCDC), and the deposition numbers are 2565270 and 2565271 for the powder structure (**3α**) and the single-crystal structure (**3β**), respectively.

3.5. Electronic Spectroscopies

UV Vis absorption spectra were measured on a UV1900 spectrophotometer by Shimadzu (Shimadzu Italia, Milan, Italy). Steady-state emission and excitation spectra were measured on an FP8500 spectrofluorimeter by Jasco (Jasco Europe, Cremella, Italy), working at a scan speed of 10,000 nm min^{-1} and data interval of 1 nm. Compounds **2** and **3** were dissolved in ethanol and placed in Suprasil® quartz cells (Hellma Italia, Milan, Italy) with 1.00 cm optical path for the measurement.

Supplementary Materials: Figure S1: ^{1}H NMR, compound **2** (DMSO-d_6, 400.2 MHz, 298 K); Figure S2: ^{13}C APT NMR, compound **2** (DMSO-d_6, 100.6 MHz, 298 K); Figure S3: ^{19}F NMR, compound **2** (DMSO-d_6, 376.6 MHz, 298 K); Figure S4: ^{1}H NMR, compound **3** (DMSO-d_6, 400.2 MHz, 298 K); Figure S5: ^{13}C APT NMR, compound **3** (DMSO-d_6, 100.6 MHz, 298 K); Figure S6: ^{19}F NMR, compound **2** (DMSO-d_6, 376.6 MHz, 298 K); Figure S7: HRMS spectrum, compound **2**; Figure S8: HRMS spectrum, compound **3**; Figure S9: IR spectrum, compound **2**; Figure S10: IR spectrum, compound **3**; Figure S11: Compound **2**, absorption (dashed line) and emission (solid line) spectra. Emission spectrum is obtained upon excitation at 297 nm. Figure S12: Compound **2**, excitation (black line) and emission spectra obtained upon excitation at 224 nm (red curve) and 297 nm (blue curve). Table S1: Crystal data, data collection and structure refinement details of structures **3α** and **3β**; Figure S13:

Packing diagram of compound **3α**; Table S2: d-spacings and squared structure factors for structure **3α**; Table S3: d-spacings and squared structure factors for structure **3β**.

Author Contributions: Conceptualization, L.Z. and G.B.G.; investigation, C.M., M.L., I.M., A.B., M.P. and C.C.; resources, L.Z., C.C. and G.B.G.; writing—original draft preparation, C.M., M.L., I.M. and G.B.G.; writing—review and editing, all authors; visualization, C.M., M.L. and I.M.; supervision and project administration, L.Z. and G.B.G. All authors have read and agreed to the published version of the manuscript.

Funding: This research received no external funding.

Data Availability Statement: The original contributions presented in this study are included in the article/Supplementary Material. Full crystallographic details of the structures reported in this paper have been deposited within the Cambridge Crystallographic Data Centre (deposition No. CCDC 2565270 and CCDC 2565271 for **3α** and **3β,** respectively) and they can be requested at http://www.ccdc.cam.ac.uk, e-mail: deposit@ccdc.cam.ac.uk, or The Director, CCDC, 12 Union Road, Cambridge, CB2 1EZ, UK.

Conflicts of Interest: C. Maestri and L. Zangirolami are employees of PRC TicinumLab Srl. C. Cavallotti is an employee of CAGE Chemicals Srl. C. Cavallotti and G.B. Giovenzana have shared ownership in CAGE Chemicals Srl. The remaining authors declare that the research was conducted in the absence of any commercial or financial relationships that could be construed as a potential conflict of interest.

Abbreviations

The following abbreviations are used in this manuscript:

ICH	International Council for Harmonisation of Technical Requirements for Pharmaceuticals for Human Use
NDSRI	Nitrosamine Drug Substance-Related Impurity
API	Active Pharmaceutical Ingredient
CYP	Cytochrome P450
EMA	European Medicines Agency
CPCA	Carcinogenic Potency Categorization Approach
FDA	Food and Drug Administration
MRM	Multiple Reaction Monitoring
DMSO	Dimethylsulfoxide
XRPD	X-Ray Powder Diffraction

References

1. Thresher, A.; Foster, R.; Ponting, D.J.; Stalford, S.A.; Tennant, R.E.; Thomas, R. Are All Nitrosamines Concerning? A Review of Mutagenicity and Carcinogenicity Data. *Regul. Toxicol. Pharmacol.* **2020**, *116*, 104749. [CrossRef] [PubMed]
2. Nudelman, R.; Kocks, G.; Mouton, B.; Ponting, D.J.; Schlingemann, J.; Simon, S.; Smith, G.F.; Teasdale, A.; Werner, A.L. The Nitrosamine "Saga": Lessons Learned from Five Years of Scrutiny. *Org. Process Res. Dev.* **2023**, *27*, 1719–1735. [CrossRef]
3. Kruhlak, N.L.; Schmidt, M.; Froetschl, R.; Graber, S.; Haas, B.; Horne, I.; Horne, S.; King, S.T.; Koval, I.A.; Kumaran, G.; et al. Determining Recommended Acceptable Intake Limits for N-Nitrosamine Impurities in Pharmaceuticals: Development and Application of the Carcinogenic Potency Categorization Approach (CPCA). *Regul. Toxicol. Pharmacol.* **2024**, *150*, 105640. [CrossRef] [PubMed]
4. Vogel, M.; Escher, S.E.; Weiler, E.; Londenberg, A.; Deppenmeier, U.; Whomsley, R. Quantitative Investigation of Nitrosamine Drug Substance-Related Impurities (NDSRIs) Under Artificial Gastric Conditions by Liquid Chromatography–Tandem Mass Spectrometry and Structure–Activity Relationship Analysis. *Drug Test. Anal.* **2025**, *17*, 1772–1784. [CrossRef] [PubMed]
5. Anderson, V.R.; Perry, C.M. Levofloxacin. *Drugs* **2012**, *68*, 535–565. [CrossRef] [PubMed]
6. Wimer, S.M.; Schoonover, L.; Garrison, M.W. Levofloxacin: A Therapeutic Review. *Clin. Ther.* **1998**, *20*, 1049–1070. [CrossRef] [PubMed]
7. Groom, C.R.; Bruno, I.J.; Lightfoot, M.P.; Ward, S.C. The Cambridge Structural Database. *Acta Crystallogr. B Struct. Sci. Cryst. Eng. Mater.* **2016**, *72*, 171–179. [CrossRef] [PubMed]

8. Kasha, M. Characterization of Electronic Transitions in Complex Molecules. *Discuss. Faraday Soc.* **1950**, *9*, 14–19. [CrossRef]
9. Perez, N.; Olmo, F.; Nuñez-Marinero, P.; Romay, L.; Colina, A.; Javier del Campo, F.; Heras, A. Levofloxacin Determination in Urine by Photoluminescence Spectroelectrochemistry. *Electrochim. Acta* **2025**, *539*, 147123. [CrossRef]
10. Matchette, L.S.; Agrawal, A.; Pfefer, T.J. Fluoroquinolone Antibiotics Having the Potential to Interfere with Fluorescence-Based Diagnosis. *Photochem. Photobiol.* **2007**, *83*, 1386–1393. [CrossRef] [PubMed]
11. Thakur, R.; Mallick, A.; Chakraborty, A. Photophysical and Photodynamical Study of Fluoroquinolone Drug Molecule in Bile Salt Aggregates. *Photochem. Photobiol.* **2012**, *88*, 1248–1255. [CrossRef] [PubMed]
12. Altomare, A.; Cuocci, C.; Giacovazzo, C.; Moliterni, A.; Rizzi, R.; Corriero, N.; Falcicchio, A. *EXPO2013*: A Kit of Tools for Phasing Crystal Structures from Powder Data. *J. Appl. Crystallogr.* **2013**, *46*, 1231–1235. [CrossRef]
13. Altomare, A.; Campi, G.; Cuocci, C.; Eriksson, L.; Giacovazzo, C.; Moliterni, A.; Rizzi, R.; Werner, P.E. Advances in Powder Diffraction Pattern Indexing: *N-TREOR09*. *J. Appl. Crystallogr.* **2009**, *42*, 768–775. [CrossRef]
14. *CrysAlis PRO*, version 44.85; Agilent Technologies Ltd.: Yarnton, Oxfordshire, UK, 2014.
15. Sheldrick, G.M. *SHELXT*—Integrated Space-Group and Crystal-Structure Determination. *Acta Crystallogr. A Found. Adv.* **2015**, *71*, 3–8. [CrossRef] [PubMed]
16. Dolomanov, O.V.; Bourhis, L.J.; Gildea, R.J.; Howard, J.A.K.; Puschmann, H. *OLEX2*: A Complete Structure Solution, Refinement and Analysis Program. *J. Appl. Crystallogr.* **2009**, *42*, 339–341. [CrossRef]
17. MacRae, C.F.; Sovago, I.; Cottrell, S.J.; Galek, P.T.A.; McCabe, P.; Pidcock, E.; Platings, M.; Shields, G.P.; Stevens, J.S.; Towler, M.; et al. Mercury 4.0: From Visualization to Analysis, Design and Prediction. *J. Appl. Crystallogr.* **2020**, *53*, 226–235. [CrossRef] [PubMed]